

Bearing Race and Roller Line Contact Analysis in 2D

J. Chmelar^{1,*}, V. Dynybyl¹

¹ Czech Technical University in Prague, FME, Department of Designing and Machine Components

* Jakub.Chmelar@fs.cvut.cz

Abstract: Bearing race and roller contact analysis was performed. Comparison of Hertz analytical with fem elasto-plastic solution gives very similar results of contact pressure profile and sub-surface stress development in elastic domain. When material yield occurs results become different. Johnson-Cook's constitutive material model was used for elasto-plastic material behaviour.

Keywords: Bearing; Contact; Johnson-Cook; Hertz; Subsurface stress

1 Introduction

Dominant loading mode of bearing is contact between bearing race and rolling elements. Elemental load depends on bearing inner geometry, amount of rolling elements, radial clearance, external load character and supporting structure stiffness. Identification of elemental load could be estimated using standard ISO/TS 16 281: 2008 [1], that provides bearing analysis method based on bearing mathematical model or with use of FEM bearing modelling, that is more complicated and require more time resources. Bearing reliability is dependent on bearing roller and race contact properties mainly pressure, lubrication and material. Induced sub-surface stress influences material behaviour and is responsible for sub-surface initiated damage.

2 Contact definition

Analysis is focused on line contact modelling in plane (2D). The contact is defined by parameters listed in Fig 1 - Contact bodies curvature - R_i , Material of bodies represented by Young's Modulus - E_i , Poisson's constant - ν_i and acting force per millimetre of length - P . The contact area is considered as rectangle with infinite length and width according to Fig. 2

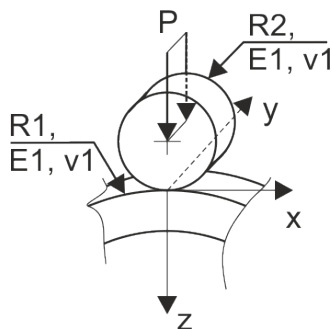


Fig. 1: Hertz line contact model definition.

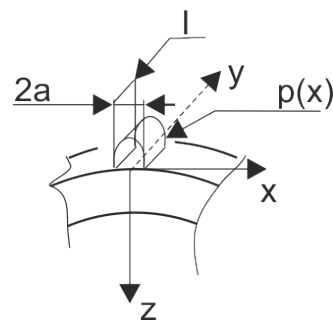


Fig. 2: Hertz line contact pressure description.

2.1 Hertz line contact analytical model

When two cylindrical non-conforming, smooth elastic bodies are forced into contact, the area that is formed in contact spot is assumed to be an infinite rectangle [2] with width according to Eq. (1)

$$a = \sqrt{\frac{4PR}{\pi E^*}} \quad (1)$$

Induced contact pressure distribution, assumed to be constant in direction of y coordinate Fig. 2, has parabolic shape described by equation Eq. (2) where the phrase in front of square root is maximal pressure [2].

$$p(x) = \frac{2P}{\pi a^2} \sqrt{(a^2 - x^2)} \quad (2)$$

In Eq. (1) and Eq. (2) are used following substitutions: mutual contact bodies curvature R and mutual Young modulus E^* . They are calculated according to equations Eq. (3) and Eq. (4) respectively.

$$\frac{1}{E^*} = \frac{1 - \nu_1}{E_1} + \frac{1 - \nu_2}{E_2} \quad (3)$$

$$\frac{1}{R} = \frac{1}{R_1} + \frac{1}{R_2} \quad (4)$$

Hertz theory is according to [2] defined with following assumptions: (i) The contact area width is small comparing to size of bodies in contact. (ii) The contact area width is small comparing to curvature of both contact bodies. (iii) Elastic - linear material behaviour. (iv) Surfaces are smooth and frictionless. (v) Plane strain conditions considered. (vi) Load is constant in off plane direction.

2.1.1 Sub-surface stress conditions

Contact of bodies induce stress response in material. The stresses could be described using potential theory [2]. For contact centre, they were simplified to following form Eq. (5) - (7). Orthogonal stresses below contact centre match principal stresses, that makes it analysis straight forward.

$$\sigma_1 = \sigma_x = -p_0 \left[\left(2 - \left(\frac{z^2}{a^2} + 1 \right)^{-1} \right) \sqrt{\frac{z^2}{a^2} + 1} - 2 \left| \frac{z}{a} \right| \right] \quad (5)$$

$$\sigma_2 = \sigma_y = -2p_0\nu \left[\sqrt{\frac{z^2}{a^2} + 1} - \left| \frac{z}{a} \right| \right] \quad (6)$$

$$\sigma_3 = \sigma_z = -p_0 \left[\sqrt{\frac{z^2}{a^2} + 1} \right]^{-1} \quad (7)$$

2.1.2 Material Yield prediction

Material Yield sub-surface could be predicted according to available yield criterion. There are two widely used when considering rolling contact fatigue [3]. Max. shear stress according to Tresca (8) and distortional energy criterion Von Mises Eq. (9). The σ_Y is material yield strength in pure tension.

$$\tau_{max} = \left| \frac{\sigma_1 - \sigma_3}{2} \right| > \frac{1}{2} \sigma_Y \quad (8)$$

$$\sigma_{vm} = \sqrt{\frac{1}{2} \left[(\sigma_1 - \sigma_2)^2 + (\sigma_1 - \sigma_3)^2 + (\sigma_2 - \sigma_3)^2 \right]} > \sigma_Y \quad (9)$$

Material yield occurs when limiting stress according to chosen criterion is exceeded. [2]. It could be proven by combining Eq. (5) - (7) to (8) or (9) respectively contact pressure for material yield could be calculated. The resulting expressions are summarized in Tab. 1.

2.2 FEM Model

FEM model of contact was assembled in Abaqus to support and enhance Hertz contact theory results in plastic domain. Standard roller bearing NU206 was used as reference geometry. Parameters are summarized in Tab. 3. The model consists of two planar bodies (3 DOF) - roller and race, forced into contact. Both bodies are driven by reference points RP1 and RP2 Fig. 3, where RP1 has constrained 2 DOFs: X - direction and RY - Rotation around Y axis. Force is applied to RP1. RP2 has all 3 DOFs constrained. Both RPs are connected with geometry by rigid beam elements.

Tab. 1: Summary of Hertz Line Contact Sub-surface stresses.

Criterion	Designation	Unit	Expression
Max. of Tresca shear stress	τ_{Tr}	$[N/mm^2]$	$0,3 p_0$
Max. Tresca shear stress depth	$z_{\tau_{Tr}}$	$[mm]$	$0,78 a$
Max. Von Mises stress	σ_{vm}	$[N/mm^2]$	$0,56 p_0$
Max. Von Mises stress depth	$z_{\sigma_{vm}}$	$[mm]$	$0,7 a$
Contact press. Tresca yield	$p_0 Y_{Tr}$	$[N/mm^2]$	$1,67 \sigma_Y$
Contact press. von Mises yield	$p_0 Y_{VM}$	$[N/mm^2]$	$1,79 \sigma_Y$

Tab. 2: Johnson-Cook material model parameters for 100Cr6 steel, 300 HV10, non-hardened. [5]

A	B	n	m
$[N/mm^2]$	$[N/mm^2]$		
688.17	150.82	0.3362	2.7786

2.2.1 Mesh

For whole model there were used planar strain quadratic elements - CPE8R [4]. The mesh is designed as structured in area of contact and where inspected sub-surface stresses were expected. The rest of model is meshed with free mesh consisting of quad elements.

2.2.2 Material

Constitutive material model Jameson-Cook was chosen. This model is based on empirical data and provides good results for isotropic materials [4]. The model is defined by Eq. (10). The advantage of this model is that it is widely used, so parameters are well accessible. In this model A - is yield stress in 0.2 % strain offset, B - is strain hardening coefficient and n - is hardening exponent. The other coefficient are not applicable for this quasi static fem analysis since they are related to time dependent dynamic strain flow in material which is not considered in this model.

$$\sigma_o = \left[A + B \overline{\varepsilon}^{pl n} \right] \left[1 + C \ln \frac{\dot{\varepsilon}^{pl}}{\dot{\varepsilon}_0} \right] \left(1 - \hat{\Theta}^m \right) \quad (10)$$

Used Johnson-Cook's material values for steel 100Cr6 in non-hardened state are summarized in 2. For elastic material behaviour Young elastic modulus $E = 210\text{GPa}$ and $\nu = 0.277$ was used.

2.2.3 Contact properties

The contact was modelled using finite sliding algorithm and surface-to-surface contact discretization. The contact was set up as frictionless with no stiffness penalty in normal direction.

Tab. 3: FEM roller bearing model geometry.

Bearing	hole dia.	Inner race dia.	Roller length	Roller dia.
	$[mm]$	$[mm]$	$[mm]$	$[mm]$
NU206	30	37.5	10	9

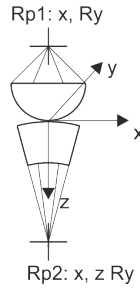


Fig. 3: Contact model with applied boundary conditions.

3 Results

There were performed calculations on FEM model for 5 different load cases expressed in contact pressure value: 0,5 GPa, 0,8 GPa, 1,3 GPa, 1,62 GPa and 2,5 GPa. Calculations were performed both for elastic and elasto plastic material model. The results are presented in following sections.

3.1 Contact pressure

Comparison of contact pressure for calculated cases are presented in Fig. 4. Calculated contact pressure (according to Tab. 1) where von Mises criterion predicts first yield in material fits the declination of line connecting discrete result points of elasto plastic material solution. Below that declination point, in elastic material model, all three solutions give similar results. In Fig. 5 contact pressure profiles of load case 1,62 GPa are compared. Elastic Hertz solution well follows FEM elastic solution. For elasto plastic material behaviour there is obvious a maximal contact pressure drop accompanied with extension of contact zone width. Assumed parabolic pressure profile of elastic solution is slightly flattered.

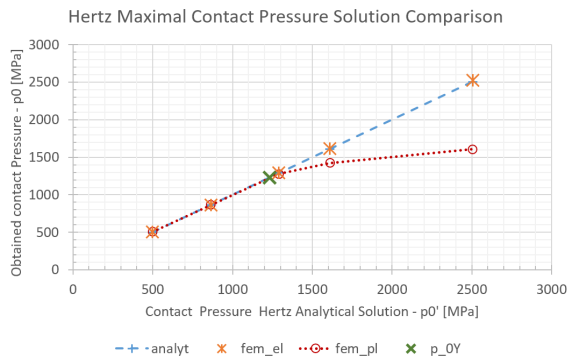


Fig. 4: Hertz contact comparison of Hertz-anal, fem-el and fem el-pl solutions in 5 load points. Green cross indicates contact pressure where first von Mises yield to occurs according to Tab. 1

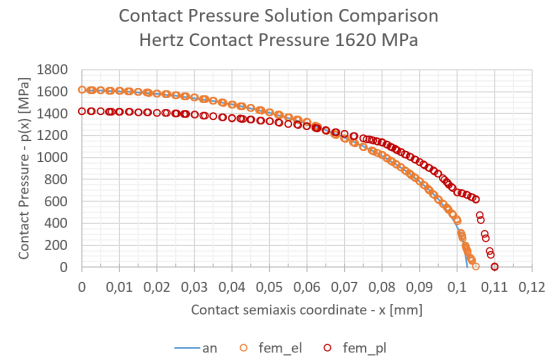


Fig. 5: Comparison of Hertz contact pressure profile for Hertz-anal, fem-el and fem el-pl solutions at cpress 1,62 GPa.

3.2 Sub-Surface stress

3.2.1 Elastic solution

Analysis of sub-surface stress field was performed. Comparison of orthogonal sub-surface principal stresses calculated according to Eq. (5) - (7) with fem solution is presented in Fig.6. Stresses and depth are normalised to maximal pressure and contact half-width respectively. It is obvious that results from both solutions with respect to small deviations caused by different solution nature agree. Presented results are valid only in elastic domain, but provides clear insight into material loading modes below contact centre. Recalculated principal stresses to Max. plane shear stress according to Tresca and von Mises stress are in Fig. 7. It can be seen that both stresses reach their maximal values in certain depth below surface. This depth could be easily estimated according to equations provided in Tab. 1.

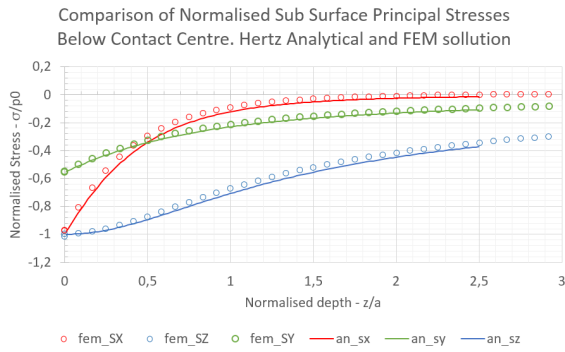


Fig. 6: Comparison of analytical and FEM principal stress development solution below centre of contact. The solution is valid only in elastic domain



Fig. 7: Normalised development of sub-surface stresses Tresca and von Mises. Analytical solution, valid only in elastic domain.

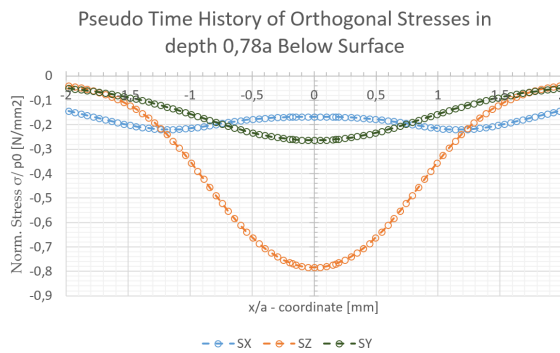


Fig. 8: History of principal stresses in depth 0.78a below surface. Point of contact at 0 point.

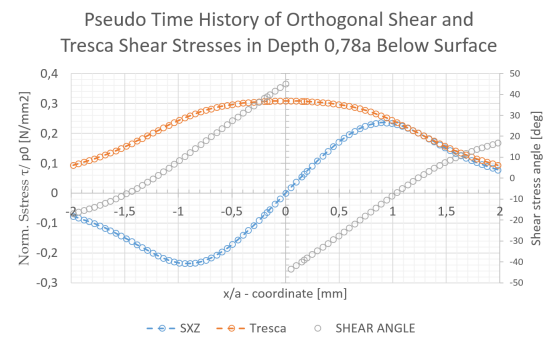


Fig. 9: History of shear stresses (Orthogonal and Tresca) in depth 0.78a below contact surface and development of Tresca shear stress angle.

The complexity of stresses below contact is well illustrated in Fig. 8 where all three orthogonal stresses are viewed. The point of contact is at zero coordinate, so when roller moves, observed point goes through all viewed stress states. It is obvious that stresses change with time unproportional. In Fig. 9 are viewed orthogonal shear stress and Tresca shear stress below surface during roller pass. It is apparent that below observed point the shear stress changes its direction by 90.

3.2.2 Elasto-plastic solution

Results from load cases beyond material yield were obtained only by FEM method. Comparison of von Mises stress obtained is in Fig. 10. Material Yield cause maximal stress value drop and induce material plastic behaviour. Progression of material plasticity with respect to applied contact pressure is viewed in Fig. 11.

4 Conclusion

The analysis of roller bearing line contact was performed. Method of analytical Hertz contact stress solution and FEM were used and compared during analysis. It was proved that analytical solution provides very efficient tool for contact analysis. It is although very important to know the limits of this method that are summarized in section 2.1. FEM was used to analyse stress field below contact. The model in FEM was built as planar with plain strain elements. Johnson-Cook material model was used to model elasto plastic material behaviour as described in 2.2.2. The contact pressure solutions are presented in Fig. 4 where is obvious material yield when higher load is applied. When material yield strength is exceeded the contact area is extended and thus there is declination of contact pressure. Parabolic contact pressure profile flatters as in Fig. 5. Comparison of sub surface principal stresses below contact centre proves FEM model Fig. 6. Von Mises stress and shear stress according to Tresca are in Fig. 7. There is no shear stress on the surface, because off plane stress component is

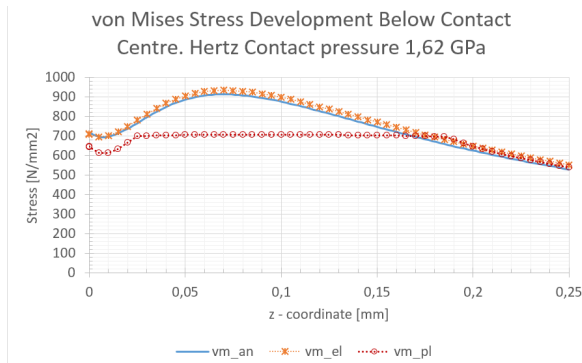


Fig. 10: Comparison of analytical and FEM principal stress development solution below centre of contact. The solution is valid only in elastic domain. $\sigma_Y = 688 \text{ N/mm}^2$.

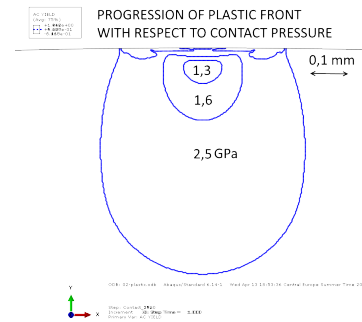


Fig. 11: Progression of material plasticity (contours delimiting areas with plastic mat. behaviour) with respect to contact pressure below contact centre. $\sigma_Y = 688 \text{ N/mm}^2$

not considered in Tresca. If analysed Von Mises stress, surface stress is calculated. Maximal values are for both reached below surface. Equations for quick estimation of these values are in Tab. 1. When stresses development is plotted for one point below surface during roller pass is obvious that complex and unproportional material stresses are present. See Fig. 8. Below contact centre the direction of principal Tresca shear stress changes rapidly, that is in Fig. 9 illustrated by Tresca shear stress angle development. Comparison of elastic material solution with plastic is in Fig. 10 where is obvious material yield limit on Von Mises's curve. The progression of plastic zone with loading is illustrated in Fig. 11. The first plastic point forms in location of Max. von Mises stress and grows.

References

- [1] ISO 16281:2008 Rolling bearings Methods for calculating the modified reference rating life for universally loaded bearings.
- [2] K. L. Johnson, Contact Mechanics, Cambridge, Cambridge University Press, 1985.
- [3] Ervin V. Zaretsky, Rolling Bearing Life Prediction Theory and Application, 2013, Available electronically at <http://www.sti.nasa.gov>.
- [4] ABAQUS 6.14 Online Documentation, Dassault Systmes, 2014.
G. Author et al., Title of Proceedings Paper, in proc.: Proceedings Title (2010), ed. A. Editor, Organizing Institution, Conference Location, 181–190.
- [5] A. Shrot, M. Baker, Is It Possible to Identify Johnson-Cook Law Parameters From Machining Simulations?, International Journal of Material Forming (2010) Vol. 3, Suppl 1, 443–446, doi: 10.1007/s12289-010-0802-4.